Sensor with enhanced performance based on photonic crystal with a defect layer

I.M. Efimov [1], N.A. Vanyushkin [1], S.S. Golik [1,2], A.H. Gevorgyan [1]
[1] School of Natural Sciences, Far Eastern Federal University,
690922, Vladivostok, Russia, Russky Island, Ajax Bay 10;
[2] Institute of Automation and Control Processes, Far East Branch,
Russian Academy of Sciences, 690041, Vladivostok, Russia

Abstract

We propose an improved structure of an optical biosensor based on a photonic crystal with a defect layer, which can detect the concentration of organic contaminants in water by defect mode shift. We investigated 4 types of defective photonic crystals with different arrangements of layers inside the perfect photonic crystals and their impact on the performance of the sensor. The sensitivity and amplitude of defect mode were examined as a function of defect layer thickness. Also, the peculiarities of edge modes in the presence of defect layer were investigated. Finally, we obtained a characteristic equation to determine the wavelengths of defect modes for an arbitrary 1D photonic crystal with an isotropic defect inside.

Keywords: sensor, photonic crystal, defect modes, organic contaminants, sensitivity

Citation: Efimov IM, Vanyushkin NA, Golik SS, Gevorgyan AH. Sensor with enhanced performance based on photonic crystal with a defect layer. Computer Optics 2023; 47(4): 572-579. DOI: 10.18287/2412-6179-CO-1245.

Acknowledgements: The work was supported by the Foundation for the Advancement of Theoretical Physics and Mathematics "BASIS" (Grant № 21-1-1-6-1).

Introduction

In the current world the development of chemical and biological industries is at an extremely high level and every year more and more compounds are synthesized. This is due to trends in the development of the industrial sector, but we should not forget about the toxicity of some of these compounds. There are compounds that are deadly to humans even at the smallest concentrations [1]. These problems dictate the need to develop methods and instruments for highly accurate detection of various contaminants even at the lowest concentrations.

Various methods for detecting substances are currently being developed [2]. In particular, optical methods of research are actively developing. Optical sensors based on photonic crystals (PCs), including those with a defect in the structure, are of great interest [3 – 26]. PCs are artificial dielectric structures with periodic refractive index modulation. In recent years, they have attracted much interest due to their unprecedented ability to control the propagation behavior of electromagnetic waves and potential applications in ultra-small all-optical integrated circuits [27]. PCs have the unique property of having a certain range of wavelengths, called the photonic bandgap (PBG), in which an electromagnetic wave cannot propagate through the PC [25]. In practice, this means that if the radiation with a wavelength inside the PBG is incident on the PC, it experiences a strong reflection from the PC. In this way the PC can act as a mirror or an optical filter. If a defect layer (DL) is added to the periodic structure of the PC, the periodicity of the structure is disrupted, causing a change in the transmission and reflection spectra throughout the spectral region. Just as the introduction of DLs into semiconductor superlattices can lead to defect states, DLs in one-dimensional PCs can also create localized defect modes (DMs) within the PBG. The position and shape of the DM depends on the parameters of the DL, such as the thickness and refractive index of the DL. It is this property that underlies our sensor. In this work, the defect is a layer composed of water with organic contaminant added. A change in the concentration of the contaminant causes a change in the refractive index of the DL, which in turn shifts the position of the DM, which can be detected by the sensor. The organic contaminant concentration in the DL is determined by this deviation.

In [28], we investigated an optical PC-based sensor with a DL. We encountered the following problem: due to the large absorption of the components of the sensor structure in the infrared range, the magnitude of the transmittance peak (DM amplitude was determined from the following form 1-R, in the case of reflection) associated with the DM excitation was too small, which limits the capability of the sensor. In this paper, to solve this problem, the operating range of the sensor was shifted to the visible region where the absorption of water, which constitutes the majority of the DL, is much lower. In addition, we optimized the sensor structure, in particular we moved to a structure with mirror symmetry and investigated the effect of DL thickness on the sensor sensitivity and DM amplitude in details. Finally, we derived the characteristic equation to determine the DM of an arbitrary PC with a defect and investigated the features of the edge modes in the presence of DL.

1. The theory

The cross-section of the PC we are considering is shown in Fig. 1.

Our structure is composed of two periodic perfect PCs with a DL between them. Each perfect PC consists of a se-

quence of N unit cells each of which is a pair of layers having thickness $h_{1,2}$ and refractive index $n_{1,2}$. The refractive indices were determined by the materials of the layers. For the selection of suitable materials, the following conditions were set: the materials should provide a high difference between the refractive indices of the n_1 and n_2, layers, be relatively inexpensive and easy to manufacture, and transparent in the spectral range of interest. The thicknesses of the layers were determined from the quarter-wave criterion $Re[n_1(\lambda_b)]h_1 = Re[n_2(\lambda_b)]h_2 = \lambda_b/4$, where λ_b is the wavelength of the center of the PBG. If this condition is met, we obtain the maximum width of the PBG.

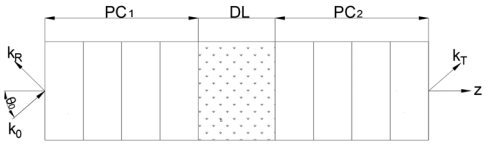

Fig. 1. Schematic diagram of the analyzed structure, k_0, k_R and k_T are the wave vectors of the incident, reflected and transmitted waves respectively, PC_1, PC_2 are the perfect PCs, θ_0 is the angle of incidence, and DL is the defect layer

The DL itself is a host medium with inclusions. The host medium is water, and the inclusions are organic contaminants. The Maxwell-Garnett effective medium approximation [29 – 30] was used to determine the refractive index of DL through the parameters of the constituent substances. This method is applicable if the macroscopic system is homogeneous and the dimensions of all particles are much smaller than the wavelength [29 – 30].

Fig. 2 shows different types of structures [31] considered in this work, which include structures with mirror symmetry (a,b,c) and without mirror symmetry (d) in relation to the DL.

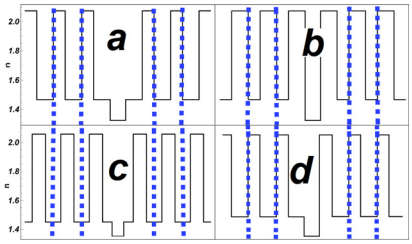

Fig. 2. Types of layer placement within the PC. The blue dashed lines show the unit cell of each perfect PC to the left and right of the DL

The structure in Fig. 2*a* (structure 1) is a case of mirror symmetry where the defect is located between two layers with lower refractive indices. The structure in Fig. 2*b* (structure 2) is a case of mirror symmetry where the defect is between two layers with a higher refractive index. The structure in Fig. 2*c* (structure 3) is a case of both mirror symmetry and symmetric unit cell, where the defect is between two layers with lower refractive indices. The structure in Fig. 2*d* (structure 4) is a case without mirror symmetry which corresponds to the structure in our earlier work [28].

In this paper we used the transfer matrix method [32 – 34] to calculate the transmission and reflection spectra of the structure under investigation.

1.1. The characteristic equation for the defected PC eigenmodes

Finding the DM can be problematic due to the high quality factor (Q-factor) of the mode, which requires calculating the reflection or transmittance spectrum of the structure with sufficiently small wavelength step size. This problem can be solved by using a characteristic equation for the DM.

The transfer matrix of a defective PC can be generally represented as:

$$m = [M_{02}M_2M_{2d}](M_d)[M_{d1}M_1M_{10}] = M_{II}M_dM_I, \quad (1)$$

where M1, Md, M_2 are "inner" transfer matrices of PC_1, DL and PC_2, i.e. these transfer matrices relate the fields at inner sides of their outer boundaries. M_{02} and M_{10} are "boundary" matrices for the interfaces between the perfect PCs and the external environment, i.e. these transfer matrices link relate the fields at different sides of the same boundary. Similarly, the matrices for the boundaries between the perfect PCs and DL are defined as M_{2d} and M_{d1}.

In the absence of absorption, any transfer matrix can be represented as [27]:

$$M = \begin{pmatrix} \frac{1}{t^*} & -\frac{r^*}{t^*} \\ -\frac{r}{t} & \frac{1}{t} \end{pmatrix}, \quad (2)$$

where r is reflection coefficient, t is transmission coefficient, the asterisks denote the complex conjugate.

In addition, since the DL is homogeneous, its inner transfer matrix can be further simplified:

$$M_d = \begin{pmatrix} e^{i\varphi} & 0 \\ 0 & e^{-i\varphi} \end{pmatrix}, \quad (3)$$

where

$$\varphi = \frac{2\pi}{\lambda} n_d h_d \cos(\theta_d),$$

and θ_d is the angle of refraction in the DL.

Now considering (2) and (3) the relation (1) turns into a matrix equation:

$$\begin{pmatrix} \frac{1}{\tau^*} & -\frac{\rho^*}{\tau^*} \\ \frac{\rho}{\tau} & \frac{1}{\tau} \end{pmatrix} = \begin{pmatrix} \frac{1}{t_{II}^*} & -\frac{r_{II}^*}{t_{II}^*} \\ \frac{r_{II}}{t_{II}} & \frac{1}{t_{II}} \end{pmatrix} \begin{pmatrix} e^{i\varphi} & 0 \\ 0 & e^{-i\varphi} \end{pmatrix} \begin{pmatrix} \frac{1}{t_I^*} & -\frac{r_I^*}{t_I^*} \\ \frac{r_I}{t_I} & \frac{1}{t_I} \end{pmatrix}. \quad (4)$$

The coefficients r, t are the reflection and transmission coefficients, index I denotes the perfect PC to the left of the defect, and index II denotes the perfect PC to the right of the defect, while τ, ρ are the reflection and transmission coefficients of the entire structure. Since the reflection coefficient ρ is zero for eigenmodes (including DM) [27], then by equating $\rho = 0$ in (4) we obtain the characteristic equation for the DM:

$$e^{2i\varphi}t_I r_{II} + r_I t_I^* = 0. \quad (5)$$

Actually, it is more convenient to use this equation in the following form:

$$e^{2i\varphi}r_{II} + r_I \frac{t_I^*}{t_I} = 0. \quad (6)$$

Equations (1 – 6) are correct if there is no absorption in the structure. When taking in to account absorption it is necessary to replace the complex conjugation in the formulas by the inversion of the wave vector $k \to -k$ [34]. Equation (6) will then take the form:

$$e^{2i\varphi}r_{II(k)} + r_{I(k)} \frac{t_{I(-k)}^*}{t_{I(k)}} = 0. \quad (7)$$

Here the values with indices k and $-k$ are calculated before and after wave vector inversion, respectively. When using the transfer matrix method, the wave vector inversion results in a change in the transfer matrices of all elements of the structure:

$$M_{\pm k} = \begin{pmatrix} \cos(\varphi) & \mp ip\sin(\varphi) \\ \pm ip\sin(\varphi) & \cos(\varphi) \end{pmatrix}, \quad (8)$$

where $p = n\cos(\theta)$, n is the refractive index of the layer considered.

In the presence of absorption, equation (6) has no real roots, but the real part of the complex root is very close to the wavelength of the DM. In addition, the imaginary part of the complex root is inversely proportional to the amplitude of the DM.

Thus, when searching for DM, one can look for the zeros of the following function:

$$f(\lambda) = \left| e^{2i\varphi}r_{II(k)} + r_{I(k)} \frac{t_{I(-k)}}{t_{I(k)}} \right|. \quad (9)$$

So, this equation we call as the characteristic one for the PC eigenmodes (including defectives one).

Fig. 3 shows the reflection spectrum of structure 2 (black) and function (8) (blue).

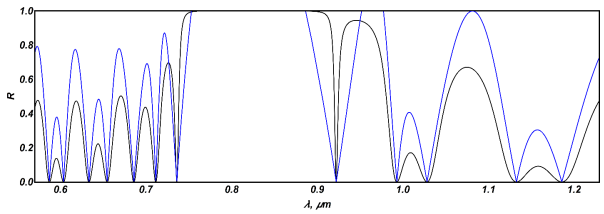

Fig. 3. Spectra of reflection (black) and function (9) (blue) for the structure 2. Parameters of structure $h_1 = 0.14$ μm, $h_2 = 0.10$ μm, $h_d = 0.44$ μm; $N = 10$

Here one can see that the obtained function has a V-shaped dip which has much broader width than the DM itself. When searching for the DM this dip is easy to detect, so this function will be used later in calculating the sensitivity of the sensor at different DL thicknesses. This method is particularly useful in the case of a very small amplitude of the DM, when the reflection minimum is barely different from 1, but the function (8) still reaches zero for the DM. It is also useful when the half-width of the DM is very small, and the DM is difficult to detect.

1.2. Peculiarities of edge modes in the presence of DL

In the absence of DL, the edge modes are equidistant in frequency, but the picture changes when DL is added. When considering different types of structures, we found the behavior of the refraction spectrum presented in Fig. 4 for the structure 2. All other types of structures demonstrate a similar dependence.

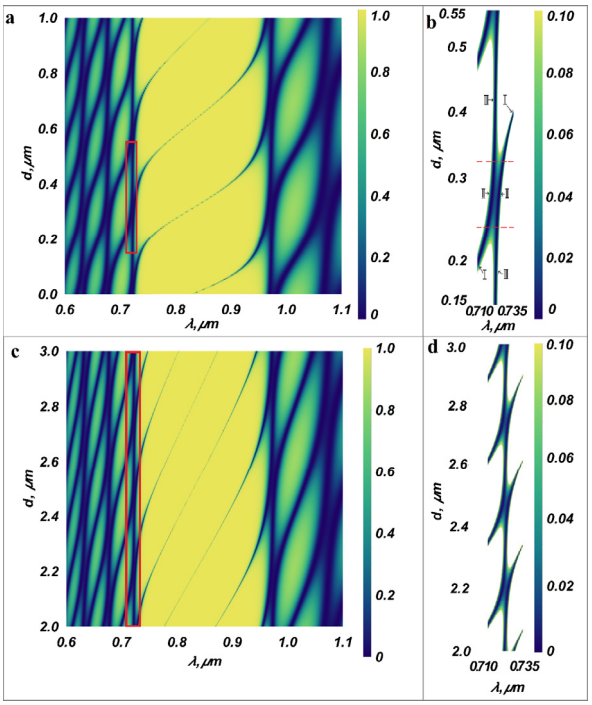

Fig. 4. (a, c) Dependence of reflection spectrum on the DL thickness for the structure 2 in different ranges of the thickness of the defective layer; (b, d) the same spectra, but zoomed in different ranges of the thickness of the defective layer. All other parameters are as in Fig. 3

Fig. 4*a* shows the dependence of reflection spectrum on the thickness of the DL. In the center, the PBG can be seen, bordering a number of edge modes on either side. The defective modes are inside the PBG, and they move as the thickness of the defective layer changes. In Fig. 4*a* when there is no defect, we still can see a mode inside the PBG, so this mode is "zeroth" mode. As the thickness of the DL increases, the following modes appear, the first, then the second one, and so on.

When considering the Fig. 4*a*, one can see that when the thickness of the DL changes the edge modes can be divided into 2 types, namely moving and stationary, and the DM refers to the moving ones. As the name implies, moving modes change their position when changing the thickness of DL, and stationary modes practically do not change their position. Let us now consider 2 zoomed in modes located next to each other in the Fig. 4b, for which 3 stages can be distinguished. Let us consider the left

mode first. At the first stage (I) one can see that edge mode experiences red shift as the DL thickness increases so we call this mode a moving one, but then at the second stage (II) the speed of movement decreases significantly. In addition, it is possible to notice that the distance between the left and right modes is almost constant here. At this stage both modes move in such a tied state, until the left mode takes the place of the former stationary mode. After this the third stage (III) starts, where the left mode becomes a stationary one. As a consequence, the mode type change occurs during the second stage. It is important to note that there is no merging of modes at the second stage. If we consider the mode on the right, it has all the same stages, but in the opposite order.

Fig. 4*c*, *d* show the dependence of reflection spectrum on the thickness of the DL at greater values of the DL thickness, when many DMs arise. As can be seen, the same behavior as above is present here. It is also worth noting that the duration of stage III (the stationary regime) is constant and does not change at larger thicknesses of DL, but the slope angle of the moving modes in stage I (including DMs) increases, and because of this the number of DMs within the PBG increases too. Let us note that we considered all the four types of the above-mentioned structures, and the said effects were found in all of them.

2. Results and discussion

To solve the main problem of the previous work [28], which was the small amplitude of the DM due to the large absorption in the infrared range, it is necessary to minimize the imaginary component of the refractive index in all components of the structure. The main component of our DL is water with a small inclusion of organic contaminant. Thus, to significantly reduce absorption, we moved the working wavelength to the visible region [35], namely around the wavelength 0.8 μm where the refractive index of water is $n_w = 1.328 + i \cdot 1.375 \cdot 10^{-7}$. Also, this wavelength is situated in the absorption minimum zone of protein compounds in the region of 0.7 – 1.1 μm [36 – 39].

To determine the refractive index function of the contamination (n_{inc}), we will use the following dielectric function (see Ref. [40])

$$\varepsilon(\omega) = \varepsilon_\infty + \sum_{i=1}^{n} \frac{s_i^2}{\omega_i^2 - \omega^2 - j\omega\gamma_1}, \qquad (10)$$

where the high-frequency constant term, $\varepsilon_\infty = 2.05$; the oscillator resonance frequency, $\omega_1 = 1098.67\ \text{cm}^{-1}$, $\omega_2 = 1025.32\ \text{cm}^{-1}$, $\omega_3 = 975.71\ \text{cm}^{-1}$, $\omega_4 = 922.95\ \text{cm}^{-1}$, and $\omega_5 = 857.57\ \text{cm}^{-1}$; the oscillator strengths, $S_1 = 46.74\ \text{cm}^{-2}$, $S_2 = 136.98\ \text{cm}^{-2}$, $S_3 = 179.70\ \text{cm}^{-2}$, $S_4 = 125.76\ \text{cm}^{-2}$, and $S_5 = 70.86\ \text{cm}^{-2}$; and the damping frequency, $\gamma_1 = 16.38\ \text{cm}^{-1}$, $\gamma_2 = 49.72\ \text{cm}^{-1}$, $\gamma_3 = 38.84\ \text{cm}^{-1}$, $\gamma_4 = 30.80\ \text{cm}^{-1}$, and $\gamma_5 = 24.70\ \text{cm}^{-1}$. Here used Drude-Lorentz approximation based on experimental data in Ref [41]. And for refractive index of the contamination, we will have $n(\omega) = \sqrt{\mu(\omega)\varepsilon(\omega)}$, with $\mu(\omega) = 1$.

In the frequency region in which we are working, the refractive index takes on an almost constant value equal to $n_{inc} = 1.432 + i \cdot 4.488 \cdot 10^{-7}$ (λ=0.8 μm), which we obtained by extrapolation in eq. (10).

For this range, a perfect PC was chosen, consisting of layers of SiO_2 and TiO_2. The refractive indices for these materials are almost constant over the selected range: $n_1 = 2.095 + i \cdot 0$ (TiO_2) and $n_2 = 1469 + i \cdot 0.0013$ (SiO_2) [42, 43]. In this paper we used N = 10 cells to the left and the same number to the right of the defective layer and considered the normal incidence of light ($\theta_0 = 0$).

Fig. 5*a* shows the difference in refractive indices of the DL components $\text{Re}(\Delta n) = |\text{Re}(n_{inc}) - \text{Re}(n_{H2O})|$, and Fig. 5*b* shows the sum of the imaginary parts of the refractive indices of all materials of our structure $\text{Im}(\Sigma n) = \text{Im}(n_{inc}) + \text{Im}(n_{H2O}) + \text{Im}(n_{SiO_2}) + \text{Im}(n_{TiO_2})$.

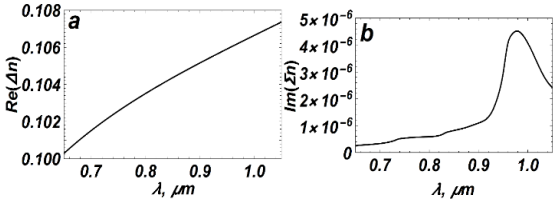

Fig. 5. (a) Difference in the refractive indices of the DL components (H_2O, organic contaminant) and (b) (b) sum of the imaginary parts of the refractive indices of all materials of our structure (H_2O, Organic inclusion, TiO_2, SiO_2)

Fig. 5*a* shows that the difference in the refractive indices of the DL components decreases in the short-wave region and Fig. 5*b* shows that the total absorption in the structure decreases in this region too.

Let us consider the reflection spectra of the structures. Fig. 6 shows the reflection spectra without DL ($h_d = 0$) for 4 types of structures (in black) and reflection spectra with DL of finite thickness (in blue).

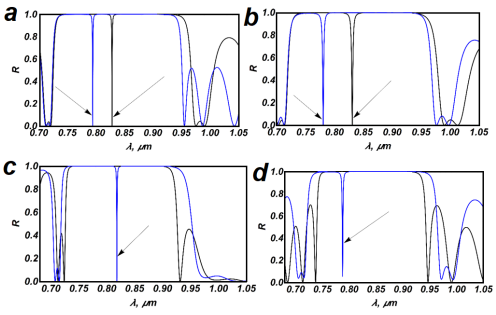

Fig. 6. Reflection spectra of 4 types of structure without a DL. (a,b) $h_1 = 0.14$ μm, $h_2 = 0.10$ μm, (black) $h_d = 0.0$ μm, (blue) $h_d = 0.25$ μm; (c) $h_1 = 0.14$ μm, $h_2 = 0.5 \cdot 2$ μm, (black) $h_d = 0.0$ μm, (blue) $h_d = 0.10$ μm; (d) $h_1 = 0.14$ μm, $h_2 = 10$ μm, (black) $h_d = 0.0$ μm, (blue) $h_d = 0.10$ μm; N = 10

The black arrow indicates DM. Note that in the cases of structures 1 (a) and 2 (b) DM is present despite of the absence of DL. This is the so-called "zeroth" mode. This is explained by the fact that in the case of mirror symmetry the periodicity of the structure in the center is broken, and this violation plays the role of a DL, so the DM appears. It is also worth paying attention to the amplitude

of the DM. One can notice that in Fig. 6d, the DM amplitude is smaller than in all the other cases. Therefore, a possible solution to the problem of low DM amplitude may lie not only in a change in the operating spectral range and structure materials, but also in the optimization of the structure geometry.

To compare the structures, it is necessary to consider the sensitivity of the biosensor with respect to changes in the refractive index of DL:

$$S_1 = \frac{d\lambda_d}{dn_d}. \qquad (11)$$

Another important parameter is the amplitude of DM, since with too small amplitude there will be no possibility to detect DM.

Fig. 7 shows sensor sensitivity (11) and DM amplitude as a function of DL thickness (for the first 3 DMs) for the structures under study. Amplitude is represented as T-1, consequently, the T-1 value is proportional to the amplitude of DM.

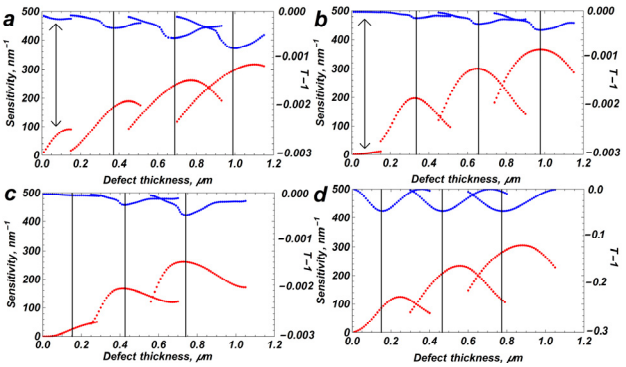

Fig. 7. Sensitivity and amplitude of the sensor as a function of DL thickness, for 4 structure types: (a) structure 1, (b) structure 2, (c) structure 3, (d) structure 4. Blue points represent DM amplitudes, red points represent sensitivity (11), black lines represent the center of the PBG. The parameters are as in Fig. 3

It should be noted that in Fig. 7*a*, *b* the "zeroth" mode is visible, it is marked with a black arrow. This mode appears due to the fact that the DM in the structures with mirror symmetry is present even in the absence of the defect, as it was mentioned above in this structure the periodicity is broken.

Let us first consider the sensitivity. In all structures we can see the increase of sensitivity with increasing DL thickness, with a general dependence, which is approximately described by the square root [44], but within each DM we can notice that the dependence of sensitivity is not monotonic. These dependencies are similar for all structures. Also, it can be seen that for the structure 2 the maximum of sensitivity is reached in the center of the PBG, while for other structures it does not take place. Overall, the second structure demonstrates the highest sensitivity among all the variants. For this structure, the sensitivity reaches 367 nm^{-1} for the third mod. It is assumed that this is since in the second structure the defect is located between two layers with a higher refractive index, which increases reflection from the borders of DL. As a consequence, the localization within the defect and the sensitivity of the DM increases.

We also investigated the effect of the number of perfect PCs on the sensitivity of the sensor. The Fig. 8 shows the dependence of sensor sensitivity on the number of perfect PCs for the second structure.

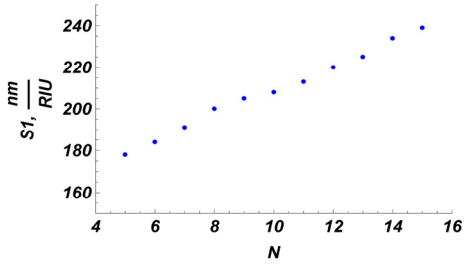

Fig. 8. Dependence of the sensor sensitivity S_1 on the number of perfect PCs for the second structure. The parameters are as in Fig. 3

It has been observed that increasing the number of layers of perfect PC increases the sensitivity of the sensor.

Now consider the amplitude. Structures 1 – 3 have much higher DM amplitude than structure 4 by 2 orders of magnitude. When considering the general dependence, the DM amplitude decreases with increasing DL thickness, which can be explained by an increase in absorption within the DL. However, for a single DM, we can observe that the changes in the DM amplitude are not monotonic, and, unlike the sensitivity, the minimum is reached in the center of the PBG for all structures. The highest amplitude is also reached at the second structure.

The second structure has the best performance among all 4 structures, so we will investigate it further. Let us now consider the sensitivity of DM to changes in the concentration of contamination.

$$S_2 = d\lambda_d / d\delta_d, \qquad (12)$$

where δ_d is volume fraction of contamination in DL.

Fig. 9*a* shows the DM shift as a function of contamination concentration, while Fig. 9*b* shows the wavelength dependence of DM as a function of concentration from 0 to 1 % with a linear approximation.

Fig. 9*a* shows the reflection spectra at different concentrations. As the contaminant concentration changes, the DM shifts to the long-wave part of the spectrum, and the Fig. 9*b* shows this shift. Similar results were obtained in a previous article [28]. A comparative characteristic is presented in Tab. 1.

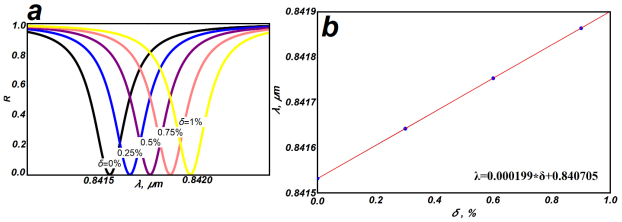

Fig. 9. (a) R spectra with changes in concentration; (b) Dependence of the DM peak on concentration; h_d = 0.325 μm. All other parameters are as in Fig. 3

It can be seen that the sensitivities are higher in structure (A), but this is due to the fact that in the previous work the DM was in the long-wavelength part of the spectrum. When considering the sensitivity normalized to the wavelength of the DM, it turns out that the new structure (B) is much more efficient. It is also worth noting that there is a significant increase in the Q-factor, which favorably affects the performance of the sensor, since it is easier to detect the shift of the DM.

Tab. 1. Comparison of characteristic of the sensor sensitivity at different parameters, (A) structure from the article [28], (B) structure 2

Structure	A	B
λ_{DM} at $\delta_i = 0$, μm	5.2930	0.84153
S_1, nm / RIU	1020	208
S_2, nm / %	1.14	0.21
S_1, λ_{DM}, 1 / RIU	0.193	0.247
S_2, λ_{DM}, 10^{-3}, 1 / %	0.210	0.250
Q-factor, $\delta = 0$	300	627

Conclusion

In conclusion, we considered an optical biosensor capable of determining the concentration of the organic contamination in water. Four basic types of geometric arrangement of the layers inside a perfect PC were considered. Variants with mirror symmetry and without mirror symmetry were considered. It was found that the variant of the structure without mirror symmetry has the lowest DM amplitude.

The highest sensitivity values are obtained for the structure with mirror symmetry where the DL is located between two layers with a high refractive index (structure 2). For this structure, the sensitivity reaches 367 nm^{-1} at a DL thickness of 0.96 μm.

It was shown that, in general, the sensitivity of the sensor increases with increasing thickness of the DL approximately as a square root (see, also [44]), but the dependence for each individual DM is nonmonotonic and reaches its maximum in the center of the PBG. The general pattern for the amplitude is the opposite, with the DM amplitude decreasing as the thickness of the DL increases. However, when considering a particular DM, the amplitude reaches its minimum in the center of the PBG and increases as it moves toward its edges.

A characteristic equation for finding the DM wavelength of an arbitrary 1D PC with a homogeneous defect inside was derived. This equation is particularly useful in finding the DM in the case of a very small DM amplitude when the reflection minimum is weakly different from 1, and DM halfwidth is very small. Let us note that this equation describes the edge mode behavior too.

The peculiarities of the edge modes in the presence of DM were investigated. It was shown that with increasing of DL thickness the edge modes and DM are moving, but there are edge modes, which practically do not change their position. The 3 stages were distinguished for each mode, in particular each mode passes a stage of a stationary mode, a coupled mode, and a moving mode. It is important to note, that in the second stage the modes do not merge and move together, as one whole.

The results of this work allow us to improve the efficiency of optical sensors based on PC with DL, including sensors (including gas sensors, or liquid sensors) and other detection devices.

Acknowledgements

The work was supported by the Foundation for the Advancement of Theoretical Physics and Mathematics “BASIS” (Grant № 21-1-1-6-1).

Conflict of interest

No potential conflict of interest was reported by the authors.

References

[1] Asghari A, Wang C, Yoo K, et al. Label-free plasmonic biosensor for rapid, quantitative, and highly sensitive COVID-19 serology: Implementation and clinical validation. Anal Chem 2021; 94(2): 975-984. DOI: 10.1021/acs.analchem.1c03850.

[2] Li G, Fan Y, Lai Y, et al. Coronavirus infections and immune responses. J Med Virol 2020; 92: 424-432. DOI: 10.1002/jmv.25685.

[3] Arano-Martinez JA, Martinez-Gonzalez CL, Salazar MI, Torres CT. A framework for biosensors assisted by multiphoton effects and machine learning. MDPI Biosens 2022; 12(9): 710-735. DOI: 10.3390/bios12090710.

[4] West RT. Development of a novel luc based s. cerevisiae biosensor. Aberdeen, UK: ProQuest; 2007: 63.

[5] Bounaas F, Labbani A. Optimized cancer cells sensor based on 1D photonic crystal vertical slot structure. Prog Electromagn Res C 2021; 117: 239-249. DOI: 10.2528/PIERC21100706.

[6] Hosseini E, Mir A, Farmani A, et al. Black phosphorous-based nanostructures for refractive index sensing with high figure of merit in the mid-infrared. Plasmonics 2022; 17: 639-646. DOI: 10.1007/s11468-021-01550-2.

[7] Asghari A, Wang C, Yoo K, et al. Fast, accurate, point-of-care COVID-19 pandemic diagnosis enabled through advanced lab-on-chip optical biosensors: Opportunities and challenges. Appl Phys Rev 2021; 8: 031313. DOI: 10.1063/5.0022211.

[8] Rende M, Xiaoping L, Hongzhong C, et al. Refractive index modulation in magnetophoresis of bioreaction induced self-assembled magnetic fluid. Opt Lett 2021; 46: 4658-4661. DOI: 10.1364/OL.435996.

[9] Shiveshwari L, Awasthi S. Transmission properties of one-dimensional ternary plasma photonic crystals. Phys Plasmas 2015; 22: 092129. DOI: 10.1063/1.4931926.

[10] Qutb SR, Aly AH, Sabra W. Salinity and temperature detection for seawater based on a 1D-defective photonic crystal material. Int J Mod Phys B 2020; 35(1): 2150012. DOI: 10.1142/S0217979221500120.

[11] Cathy M, Gareth J, et al. On-chip cavity-enhanced absorption spectroscopy using a white light-emitting diode and polymer mirrors. Lab on a Chip 2015; 15: 711-717. DOI: 10.1039/C4LC01264J.

[12] Akhilesh K, Charusluk V, et al. VOC biomarker monitoring for diabetes through exhaled breath using Ag/P-TiO2

composite plasmonic sensor. IEEE Sens J 2021; 21(20): 22631-22637. DOI: 10.1109/JSEN.2021.3104766.
[13] Akhilesh K, Vinod K, et al. SPR based optical fiber refractive index sensor using silver nanowire assisted CSMFC. IEEE Photon Technol Lett 2020; 32(8): 465-468. DOI: 10.1109/LPT.2020.2980470.
[14] Nunzio C, et al. Proof of concept for a quick and highly sensitive on-site detection of SARS-CoV-2 by plasmonic optical fibers and molecularly imprinted polymers. Sensors 2021; 21(5): 1681. DOI: 10.3390/s21051681.
[15] Muhammad U, Menal K. SARS-CoV-2 Detection using optical fiber based sensor method. Sensors 2022; 22(3): 751. DOI: 10.3390/s22030751.
[16] Kneipp J. Interrogating cells, tissues, and live animals with new generations of surface-enhanced Raman scattering probes and labels. J ACS Nano 2017; 11(2): 1136-1141. DOI: 10.1021/acsnano.7b00152.
[17] Singh S, et al. Impacts of introducing and lifting nonpharmaceutical interventions on COVID-19 daily growth rate and compliance in the United States. Proc Natl Acad Sci USA 2021; 118(12): e2021359118. DOI: 10.1073/pnas.2021359118.
[18] Monkawa A, Takimoto Y, Nakagawa T, et al. Ultra-highly sensitive detection of influenza virus by localized surface-plasmon resonance sensor. Res Square 2021; 1: 1-17. Source: <https://assets.researchsquare.com/files/rs-879879/v1/07758a1a-f369-4474-b7e7-49748057a9b7.pdf?c=1635916242>. DOI: 10.21203/rs.3.rs-879879/v1.
[19] Henriquez L, Acuna M, Rojas A. Biosensors for the detection of bacterial and viral clinical pathogens. Sensors 2020; 20(23): 6926. DOI: 10.3390/s20236926.
[20] Samson R, Navale R, Dharne S. Biosensors: frontiers in rapid detection of COVID-19. Biotech 2020; 10: 385. DOI: 10.1007/s13205-020-02369-0.
[21] Chaves F, Elsayed A, Mehaney A, et al. Defect mode modulation for a protein solution cavity surrounded by graphene and nanocomposite layers. Optik 2021; 242: 167161. DOI: 10.1016/j.ijleo.2021.167161.
[22] Taya A, Daher G, Colak I. Highly sensitive nano-sensor based on a binary photonic crystal for the detection of mycobacterium tuberculosis bacteria. J Mater Sci Mater Electron 2021; 32(1): 28406-28416. DOI: 10.1007/s10854-021-07220-7.
[23] Joannopoulos JD. Photonic crystals: Molding the flow of light. Princeton: Princeton University Press; 1995.
[24] Shkondin E, Takayama O, Aryaee Panah ME, et al. Large-scale high aspect ratio Al-doped ZnO nanopillars arrays as anisotropic metamaterials. Opt Mater Express 2017; 7(11): 1606-1627. DOI: 10.1364/OME.7.001606.
[25] Tinga WR, Voss WAG, Blossey DF. Generalized approach to multiphase dielectric mixture theory. J Appl Phys 1973; 44: 3897. DOI: 10.1063/1.1662868.
[26] Sarkar S, Gupta V, Kumar M, et al. Hybridized guided-mode resonances via colloidal plasmonic self-assembled grating. ACS Appl Mater Interfaces 2019; 11(14): 13752-13760. DOI: 10.1021/acsami.8b20535.
[27] Belyakov V. Diffraction optics of complex-structured periodic media. 2nd ed. Cham, Switzerland: Springer Nature Switzerland AG; 2019. ISBN: 978-3-319-43481-0.
[28] Efimov IM, Vanyushkin NA, Gevorgyan AH, Golik SS. Optical biosensor based on a photonic crystal with a defective layer designed to determine the concentration of SARS-CoV-2 in water. Physica Scripta 2022; 97(5): 055506. DOI: 10.1088/1402-4896/ac5ff7.
[29] Markel V. Introduction to the Maxwell Garnett approximation: tutorial. J Opt Soc Am A 2016; 33(7): 1244-1256. DOI: 10.1364/JOSAA.33.001244.
[30] Bordo V. Theory of light reflection and transmission by a plasmonic nanocomposite slab: Emergence of broadband perfect absorption. arXiv Preprint. 2021. Source: <https://arxiv.org/abs/2101.09681>.
[31] Efimov IM, Vanyushkin NA, Gevorgyan AH. Peculiarities of the electromagnetic field distribution inside a 1D photonic crystal with a defect layer. Bull Russ Acad Sci: Phys 2022; 86(1): S60-S65. DOI: 10.3103/S1062873822700393.
[32] Yeh P. Optical waves in layered media. New York: Wiley; 1988.
[33] Yariv A, Yeh P. Optical waves in crystals. New York: Wiley; 1984.
[34] Vanyushkin NA, Gevorgyan AH, Golik SS. Scattering of a plane wave by an inhomogeneous 1D dielectric layer with gradient refractive index. Opt Mater 2022; 127: 112306. DOI: 10.1016/j.optmat.2022.112306.
[35] Hale G, Querry M. Optical constants of water in the 200-nm to 200-μm wavelength region. Appl Opt 1973; 12(3): 555-563. DOI: 10.1364/AO.12.000555.
[36] Ermolinskiy P, et al. Red blood cell in the field of a beam of optical tweezers. Quantum Electron 2022; 52(1): 22-27. DOI: 10.1070/QEL17962.
[37] Cross T, Opella S. Solid-state NMR structural studies of peptides and proteins in membranes. Curr Opin Struct Biol 1994; 4(4): 574-581. DOI: 10.1016/S0959-440X(94)90220-8.
[38] Harlepp S, et al. Hemodynamic forces can be accurately measured in vivo with optical tweezers. Mol Biol Cell 2017; 28(23): 3252-3260. DOI: 10.1091/mbc.e17-06-0382.
[39] Rowe D, et al. Complex refractive index spectra of whole blood and aqueous solutions of anticoagulants, analgesics and buffers in the mid-infrared. Sci Rep 2017; 7(1): 7356. DOI: 10.1038/s41598-017-07842-0.
[40] Li D, Zhou H, Hui X, et al. Plasmonic biosensor augmented by a genetic algorithm for ultra-rapid, label-free, and multifunctional detection of COVID-19. Anal Chem 2021; 93(27): 9437-9444. DOI: 10.1021/acs.analchem.1c01078.
[41] Valerio G, Maneesh N, Leal L, et al. Ultrarapid on-site detection of SARS-CoV-2 infection using simple ATR-FTIR spectroscopy and an analysis algorithm: High sensitivity and specificity. Anal Chem 2021; 93(5): 2950-2958. DOI: 10.1021/acs.analchem.0c04608.
[42] Gao L, Lemarchand F, Lequime M. Refractive index determination of SiO2 layer in the UV/Vis/NIR range: spectrophotometric reverse engineering on single and bi-layer designs. J Eur Opt Soc Rapid Publ 2013; 8: 3010. DOI: 10.2971/jeos.2013.13010.
[43] Sarkar S, Gupta V, Kumar M, Schubert J, Probst PT, Joseph J, König TAF. Hybridized guided-mode resonances via colloidal plasmonic self-assembled grating. ACS Appl Mater Interfaces 2019; 11(14): 13752-13760. DOI: 10.1021/acsami.8b20535.
[44] Zaky A, et al. Gas sensing applications using magnetized cold plasma multilayers. Opt Quantum Electron 2022; 54(4): 217-230. DOI: 10.1007/s11082-022-03594-y.

Authors' information

Ilya Mikhailovich Efimov (b. 1996) received his bachelor's and master's degrees in Chemical Engineering from the Far Eastern Federal University, in 2018 and 2020, respectively. In 2020, he joined the Far Eastern Federal University,

Vladivostok, Russia, where he is currently a lecturer. He has authored and co-authored over 10 conference and journal refereed papers. E-mail: *efimov.im@dvfu.ru* .

Nikolay Aleksandrovich Vanyushkin (b. 1995) received the bachelor's and the master's degree in Applied Mathematics and Physics from the Moscow Institute of Physics and Technology, Moscow, Russia, in 2018 and 2020, respectively. He was with NTO IRE-Polus, Fryazino, Russia, as a research intern from 2017 to 2020. He joined the Far Eastern Federal University, Vladivostok, Russia, in 2021, where he is currently a research engineer. He has authored and co-authored over 10 conference and journal refereed papers. E-mail: *vaniuschkin.nick@ya.ru* .

Sergey Sergeevich Golik (b. 1979) graduated from Physics faculty, Far Eastern State University (now Far Eastern Federal University), Ph. D. in Physics and Mathematics, Associate Professor. He is a leading researcher at the General and Experimental Physics department, Far Eastern Federal University, a senior researcher at IAPU FEB RAS. Research interests: laser spectroscopy, nonlinear optics, photonics. E-mail: *golik.ss@dvfu.ru* .

Ashot Harutyunovich Gevorgyan (b. 1958) received the Ph.D. degree in Physics from Yerevan State University, Yerevan, Armenia, in 1987 and doctor of science 2010. He is the author of more than 185 scientific papers in peer-reviewed journals indexed in Scopus/Web of Science (the total number of his scientific and educational works is more than 310). He also has a rich experience in educational activities: he worked for 37 years as an assistant and associate professor at General Physics department at Yerevan State University, since 2010 as a professor of the department, and in 2018-2019 he headed this department. He joined the Far Eastern Federal University, Vladivostok, Russia, in 2019, where he is currently a professor. E-mail: *agevorgyan@ysu.am* .

Received October 23, 2022. The final version – December 20, 2022.